



Contents lists available at ScienceDirect

Journal of Orthopaedic Translation

journal homepage: www.journals.elsevier.com/journal-of-orthopaedic-translation

ORIGINAL ARTICLE

Molecular mechanisms of osteogenesis and antibacterial activity of Cu-bearing Ti alloy in a bone defect model with infection *in vivo*Jun Yang^{a,c,1}, Hanjun Qin^{a,1}, Yu Chai^a, Ping Zhang^a, Yirong Chen^a, Ke Yang^b, Min Qin^d, Yifang Zhang^e, Hong Xia^{c,***}, Ling Ren^{b,**}, Bin Yu^{a,*}^a Department of Orthopaedics, Nanfang Hospital, Southern Medical University; Guangdong Provincial Key Laboratory of Bone and Cartilage Regenerative Medicine, Nanfang Hospital, Southern Medical University, Guangzhou 510515, Guangdong, China^b Institute of Metal Research, Chinese Academy of Sciences, Shenyang 110016, China^c Department of Orthopaedics, Guangzhou General Hospital of Guangzhou Military Command of PLA, Guangdong Key Lab of Orthopaedic Technology and Implant Materials, Key Laboratory of Trauma & Tissue Repair of Tropical Area of PLA, Guangzhou 510010, China^d School of Public Health, Experimental Teaching Center of Preventive Medicine, Southern Medical University, Guangzhou 510515, Guangdong, China^e Editorial Office, Chinese Journal of Orthopaedic Trauma, Nanfang Hospital, Southern Medical University, Guangzhou 510515, Guangdong, China

ARTICLE INFO

Keywords:

Antibacterial
Bone defect
isobaric tags for relative and absolute quantification (iTRAQ) analysis
Osteogenesis
Ti6Al4V-6.5wt%Cu alloy

ABSTRACT

Objective: The antibacterial activity of copper (Cu)-alloy biomaterials has shown a great potential in clinical application. Here, we evaluated the osteogenesis and antibacterial effects of Ti6Al4V-6.5wt%Cu alloy in an *in vivo* model of infected bone defects and determine their responsible proteins and pathways using proteomics.**Methods:** After bone defects were filled with Ti6Al4V and Ti6Al4V-6.5wt%Cu implants for 6 week, the tissue and bone samples around the implants were harvested for radiographic, micro-CT, histological, and bone-related gene expression analyses. An iTRAQ-based protein identification/quantification approach was used to analyze the osteogenic and antibacterial effects of Ti6Al4V-6.5wt%Cu alloy.**Results:** Imaging and histological results showed Ti6Al4V alloy induced a stronger inflammatory response than Ti6Al4V-6.5wt%Cu alloy; imaging results and osteogenic protein levels showed Ti6Al4V-6.5wt%Cu alloy exerted a stronger osteogenic effect. *In vitro* experiment, we found the Ti6Al4V-6.5wt%Cu had significant antibacterial effects and inhibited the activity of *Staphylococcus aureus* in the early stage. In addition, the bacterial biofilm formed in Ti6Al4V-6.5wt%Cu group was significantly lower than that in Ti6Al4V group. Proteomic screening of 4279 proteins resulted in 35 differentially expressed proteins for further examination which were mainly associated with the cellular process, metabolic process, stimulus response, and cellular component organization. In further exploration of the mechanism of osteogenic mineralization of Ti6Al4V-6.5wt%Cu alloy, we found out SDC4 and AGRN were the top two target proteins associated with osteogenic differentiation and bone mineralization.**Conclusion:** Ti6Al4V-6.5wt%Cu alloy shows a great potential as a bone implant material due to its positive effects against bacterial infection and on bone formation.**The Translational potential of this article:** At present, titanium alloys and other non-antibacterial metal materials are used in orthopedic internal fixation operations. Our study demonstrates that Ti6Al4V-6.5wt%Cu alloy has good antibacterial and osteogenic effects *in vivo* and *in vitro*. This means that Ti6Al4V-6.5wt%Cu alloy may become a

Abbreviations: micro-CT, microcomputed tomography; iTRAQ, isobaric Tags for Relative and Absolute Quantitation; SDC4, Syndecan 4; AGRN, Agrin; XRD, X-Ray Diffraction; SEM, scanning electron microscope; UV, ultraviolet; S. Aureus, staphylococcus aureus; EDTA, Ethylene Diamine Tetraacetic Acid; ALP, alkaline phosphatase; OCN, osteocalcin; OPN, osteopontin; hBMSCs, human bone marrow stromal cells; PPI, protein-to-protein interacting; SCX, Strong Cation Exchange; LC, Liquid Chromatography; ESI, Electrospray Ionization; pAGC, predictive Automatic Gain Control; cfu, colony-forming unit; BV, bone volume; TV, tissue volume; Tb.N, trabecular number; Tb.Th, trabecular thickness; Tb.Sp, trabecular separation; DEPs, differentially expressed proteins.

* Corresponding author.

** Corresponding author.

*** Corresponding author.

E-mail addresses: qinhanjun2020@smu.edu.cn (H. Qin), gzxiahong2@126.com (H. Xia), lren@imr.ac.cn (L. Ren), yubin@smu.edu.cn (B. Yu).¹ Jun Yang and Hanjun Qin are contributed equally to this work.<https://doi.org/10.1016/j.jot.2020.10.004>

Received 30 April 2020; Received in revised form 3 October 2020; Accepted 8 October 2020

2214-031X/© 2020 The Author(s). Published by Elsevier (Singapore) Pte Ltd on behalf of Chinese Speaking Orthopaedic Society. This is an open access article under

the CC BY-NC-ND license (<http://creativecommons.org/licenses/by-nc-nd/4.0/>).

new kind of antimicrobial metallic material as internal fixation material to continuously exert its antimicrobial effects and reduce the infection rate after clinical internal fixation.

Introduction

There are 2 million cases of nosocomial infections worldwide each year, of which about 50% are related to internal fixation implants. Treatment of infected bone defects is a major challenge for clinicians. Metallic materials are frequently used for bone grafts. Despite strict sterilization and aseptic procedures, clinical experience has shown that serious bacterial infections occasionally occur [1]. Bacterial infection is among the most prevalent and serious complications of bone reconstruction surgery [2]. Bacterial contamination of surfaces leading to biofilm formation can cause infection and inflammation, such as prosthetic joint infection, which may result in implant failure [3,4]. Therefore, it is important to develop a metallic material that has both antibacterial and osteogenic effects [5].

Studies have shown that a good implant biomaterial for orthopedics should possess fundamental properties such as mechanical and biological compatibility and enhanced wear and corrosion resistance in a biological environment [6]. In addition, there has been an increasing interest in effective bone reconstruction with antibacterial activity for healthy bone growth [7]. Antimicrobial properties on medical metal can be achieved by two main approaches. The first technique is deposition of antibacterial reagents directly onto the metal surface, such as sputter coating and ion beam assisted surface modification [8–11]. The second method is direct incorporation of antibacterial reagents into the materials. There is a growing body of evidence recognizing the importance of the antibacterial function of copper (Cu). More recent attention has focused on the bactericidal function in smelting preparation of an overall type of copper materials [12,13].

In a previous study, Cu was directly incorporated into Ti6Al4V alloy to prepare a new Ti6Al4V–Cu alloy which demonstrated better comprehensive properties like high strength, excellent ductility, corrosion resistance and substantial antibacterial and antibiofilm performance as well [15,16]. A key aspect of Ti6Al4V–xCu is its antibacterial and antibiofilm performance *in vitro*. However, *in vivo* antibacterial functions are complex.

Protein adsorption has a pivotal role in the interaction between biomaterials and cells or tissues. Protein adsorption on the material surface is the very first event of this interaction, determinant for the subsequent processes like cell growth, differentiation, and extra-cellular matrix formation [17]. Understanding the link between proteins and biomaterials can improve the biomaterials for medical application [18]. Proteomic analyses hold the promise of tackling the complexity of materials and understanding correlations between material properties and their effects on complex biological systems. However, no study has investigated the antibacterial effect of Ti6Al4V–Cu alloy on bone using a proteomic approach.

Therefore, we evaluated the antibacterial performance of this new copper-containing antimicrobial metallic material *in vivo*. We also used proteomics to preliminarily explore the effect of this material on bone tissue. The significance and originality of this study is that the relationship between Ti6Al4VCu alloy and proteins has been discussed for the

first time and the mechanism of Ti6Al4VCu alloy for promoting osteogenesis and antibacterial function *in vivo* preliminarily expounded. Our results may provide a theoretical basis for the clinical application of this new copper-containing antimicrobial metallic material.

Methods

Material preparation

Cu-containing Ti6Al4V alloy was prepared by a 25 kg vacuum consumable melting furnace. The alloy ingot was hot-forged and hot-rolled into round bars with 12 mm in diameter. After hot-processing, the alloy was annealed at a temperature of 740°C before cooling in air for a duration of 1 h. The commercial medical Ti6Al4V bar was used as control. The chemical compositions of Ti6Al4V–6.5Cu and Ti6Al4V alloys are listed in Table 1. The XRD (Rigaku D/max 2500 pc) patterns and SEM (SHIMADZU SSX-550) micro-structures of Ti6Al4V–6.5Cu and Ti6Al4V alloys are shown in Fig. 1. It was found that Ti6Al4V–6.5Cu alloy was composed of equal-axed α +Ti₂Cu+ β phases (Fig. 1A and B) and Ti6Al4V alloy of equal-axed α + β phases (Fig. 1C and D).

In vitro experiments

Biofilm formation

Coculture of *Staphylococcus aureus* with alloy materials *in vitro* was performed for 3, 6, 12, 24, 48 and 96 h, respectively, at a bacterial concentration of 1×10^5 cfu/ml. The surface of the material was rinsed by water injection for three times before dried with absorbent paper. The specimens were placed onto a glass slide and stained with calcium fluoride and potassium hydroxide for 1 min before observation under UV light at $\times 100$ –400 magnification.

Detection of live and dead bacteria by confocal laser scanning microscopy

SYTO9 and PI in the SYTO9® and PI LIVE/DEAD® Bac Light™ Bacterial Viability Kit (Invitrogen, USA) were mixed at a 1:1 ratio while protected from light. The final concentrations were 10 and 60 μ mol/L. Metallic materials were cocultured with 1×10^5 cfu/ml of clinically pathogenic *S. Aureus* (ATCC25923) for 3, 6, 12, 24, and 48 h. The surface of the material was rinsed with water three times and dried with absorbent paper. The specimen was placed onto a glass slide and 9 μ l fluorescent dye solution was added to cover the material surface, followed by incubation in the dark for 15 min. The fluorescent dye SYTO9 caused the live bacteria to emit green fluorescence while PI caused dead bacteria to emit red fluorescence. A laser scanning confocal microscope was used to observe the bacterial biofilm with excitation at 488 nm and a 505–550 nm filter for SYTO9 green fluorescence and a 650 nm filter to observe the red fluorescence of PI. Three visual fields were randomly selected for observation in each specimen, marked as v1–v3, and the green fluorescence intensity (Fg) and red fluorescence intensity (Fr) of each visual field were recorded.

Table 1
Chemical compositions of Ti6Al4V–6.5wt.%Cu and Ti6Al4V alloys.

Group	Element								
	Al	V	Cu	Fe	C	N	O	H	Ti
Ti6Al4V–6Cu	5.70	3.78	6.5	0.1	0.011	0.002	0.09	0.002	Balance
Ti6Al4V	6.01	3.97	\	0.02	0.01	0.001	0.03	0.001	Balance

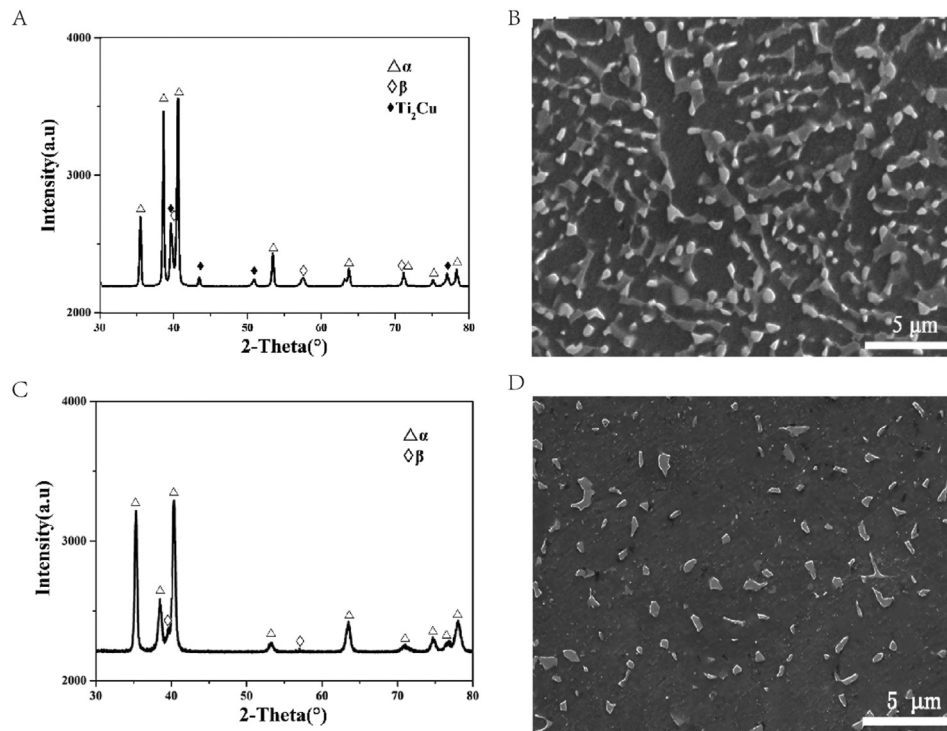


Fig. 1. (A) The XRD patterns of annealed Ti6Al4V-6.5Cu alloy and (B) the corresponding SEM images; (C) the XRD patterns of annealed Ti6Al4V alloy and (D) the corresponding SEM images.

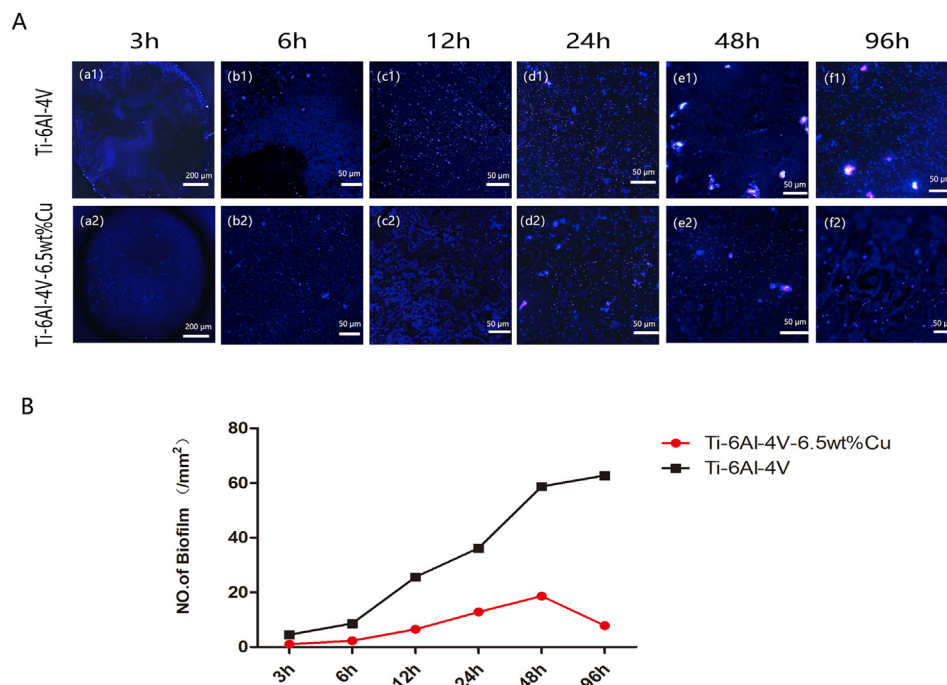


Fig. 2. (A) The biofilms in Ti6Al4V group and Ti6Al4V-6.5wt% Cu group exhibited typical fluorescence images in 3 (a1-a2), 6 (b1-b2), 12 (c1-c2), 24 (d1-d2), 48 (e1-e2), and 96 h (f1-f2). (B) Quantitative analysis of biofilm fluorescence.

In vivo experiments

Establishment of animal models of an infected bone defect and alloy material implantation

Models of a single cortical bone defect were created using SD rats with an age of 3 months and a weight of 400–450 g purchased from Southern Medical University (Guangzhou, China). A cylinder was used as the

critical diameter of the single cortical bone defect. As a preliminary experiment found that a bone defect of 2–3 mm in diameter could not meet the needs of an animal model of infected bone defects during a 6-week period, a cylinder with a diameter of 4 mm and thickness of 2 mm was selected as the model of a single cortical bone defect in this study (graphical abstract).

Anesthesia was induced by intraperitoneal injection of ketamine (60

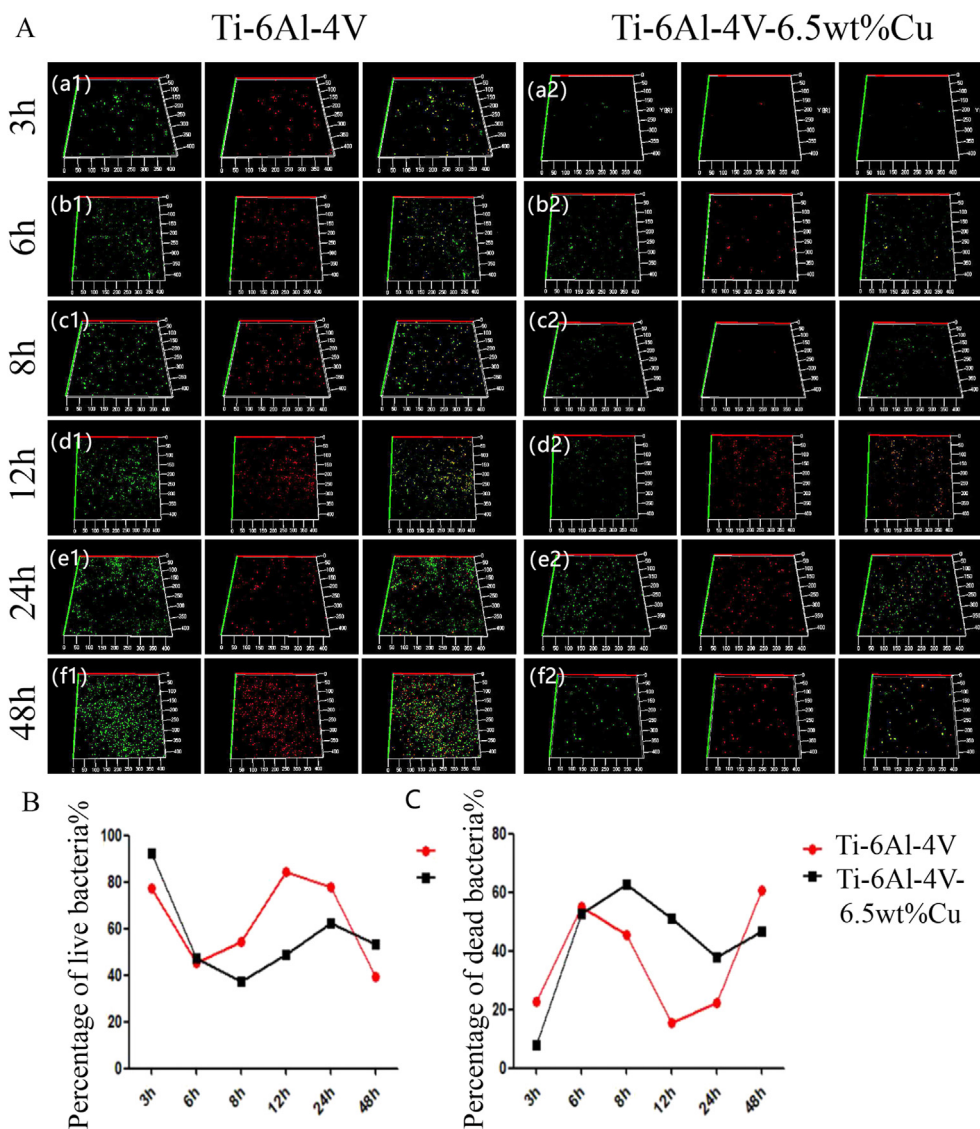


Fig. 3. (A) Detection of percentages of dead and live bacteria by confocal laser scanning microscopy. 3D reconstructed images of *S. aureus* after direct contact with Ti6Al4V alloy and Ti6Al4V-6.5wt%Cu alloy for 3 (a1-a2), 6 (b1-b2), 8 (c1-c2), 12 (d1-d2), 24 (e1-e2), and 48 h (f1-f2) for evaluation of antibacterial activity. (B) Percentages of live *S. aureus* at 3, 6, 8, 12, 24, and 48 h for the two groups. (C) Percentages of dead *S. aureus* at 3, 6, 8, 12, 24, and 48 h for the two groups.

mg/kg body weight), xylazine (6 mg/kg body weight), and atropine (0.1 mg/kg body weight). The proximal tibia was then exposed by a medial longitudinal incision. A 4 mm (diameter) × 2 mm (thickness) hole was made near the proximal tibia and 5 mm below the knee joint. A bacterial suspension (50 μL) containing 1×10^5 cfu/ml *S. aureus* was injected into the bone defect site.

Animal models were randomly divided into 3 even groups (n = 6 per group): a sham group (a model of a simple bone defect which was subjected to no implantation or infection), a control group subjected to implantation of Ti6Al4V alloy (Φ = 4 mm) into the infected defects, and an experimental group subjected to implantation of Ti6Al4V-6.5wt%Cu alloy (Φ = 4 mm) into the infected defects. The animal experiment was reviewed and approved by the Institutional Animal Care and Use Committee of the Southern Medical University, Guangzhou, China.

General observations

No antibiotics were administered after surgery. Observation of wound healing (red and/or swollen area, and skin ulceration) and local skin temperature measurements were performed once daily for 6 weeks. Local skin temperature was measured by an electronic thermometer. A continuous 7-day measurement of local skin temperature was conducted.

Temperature measurements were repeated five times and averaged. Bacterial secretions in the incision were identified by microbiological detection. Blood samples were collected from the heart of each animal to detect changes in erythrocytes, leukocytes, neutrophils, blood platelets, hemoglobin, and C-reactive protein at 72 h post-operation. Collection of blood via the heart was performed in a manner that ensured an adequate blood volume (5 ml) was obtained from the rats.

Radiographic analyses

To observe healing of the bone infection, we acquired radiographic images. X-ray images of both lower limbs were obtained. The appearance of the bone and joint destruction, bone resorption, osteolysis, periosteal thickening, and bone separation were considered as signs of bone infection.

Continuous micro-CT cross-sectional images were obtained in the 10-mm region surrounding the center of the bone defect. The specimen was fixed in the test tube of the micro-CT system and scanned along the long axis of the specimen at a resolution of 12 μm. To reduce interference by surrounding structures in micro-CT scanning, the following scan parameters were used: voltage, 70 kV; current, 141 A; pixel size, 9.485 μm; rotating scanning range, 180°. Selected images were imported into

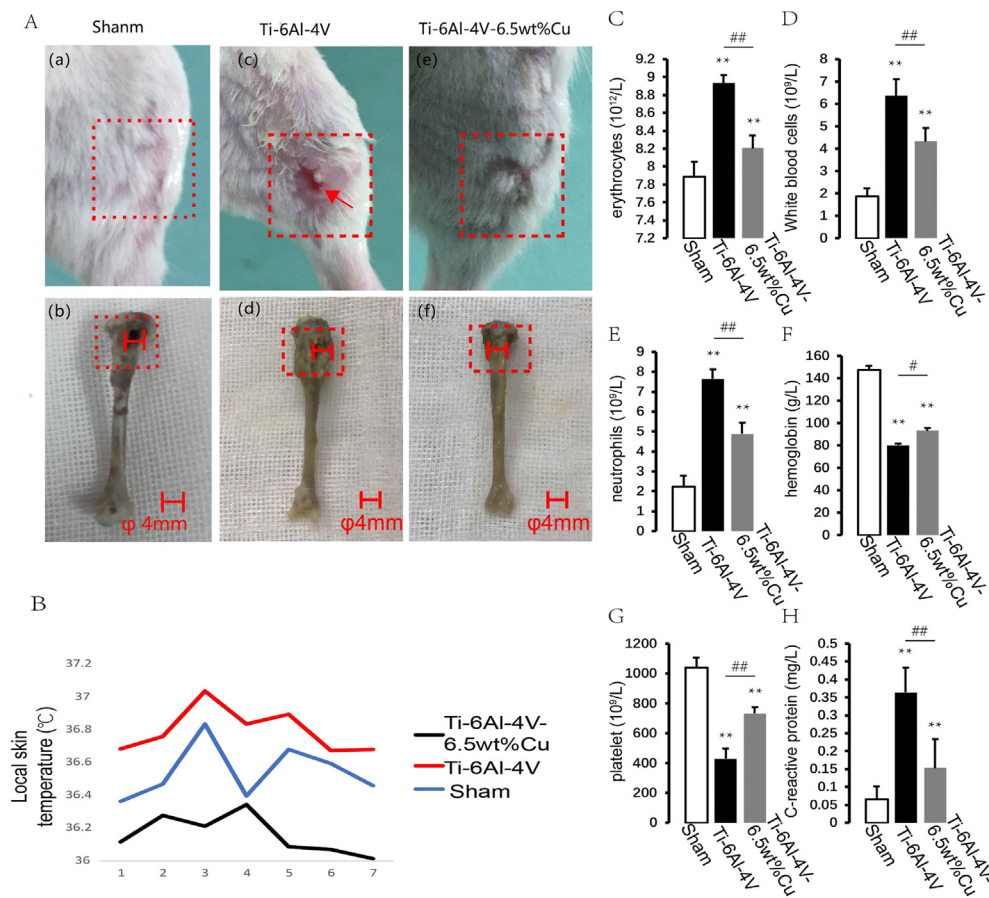


Fig. 4. A (a, b, c, d e and f) Clinical evaluation of bone infection and nonunion after 2 weeks. Signs of soft tissue infection in lower limbs: leg swelling, skin ulcer, pus formation, and yellow fluid exudation. (B) Evaluation of body surface temperature. The local skin temperature in the control group was significantly higher than in the experimental group and sham group. Process of a bone defect triggering a body stress response. (C, D) Erythrocytes and white blood cells. (E, H) Numbers of C-reactive protein and neutrophils. (F, G) Hemoglobin and platelets. These results indicated that the inflammatory reaction in the control group was more intense than in the experimental group. Results of blood tests. n = 5 per group. *p < 0.05 compared with sham, **p < 0.01 compared with sham.

Mimics software, and grayscale values of the tibial cortical and trabecular bones were used as a reference to select the appropriate gray scale range of bone. The bone in the target area was then reconstructed to obtain 3D images.

The number and structure of new bone formations, inflammatory changes in bone tissue, and changes in the medullary cavity and bone surrounding the tibial bone defect were observed using micro-CT software. Bone destruction, cortical dissolution, and resorption were identified as signs of bone infection. Measurement of the bone area by micro-CT was used to calculate the average value of the cross-sectional area of bone.

Effect of copper ions on animal organs observed by copper salt staining

Animals were sacrificed at 6 weeks and their viscera (heart, liver, spleen, and kidneys) were removed. Tissue sections were prepared after soaking in a 4% polyformaldehyde solution. The tissue sections were stained with dithiooxamide in a 37°C water bath for 16–48 h. Then, the tissue sections were rinsed with 70% ethanol, followed by distilled water, and dried. Nuclei were stained with solid red stain for 1 min. Then, a copper salt stain, including red acid and copper salt, was used to analyze the effects of copper ions on animal organs. The red amino acid stain was prepared by mixing 2 ml red amino acid solution with 48 ml dith oxidant. Positivity was defined as black deposits.

Histological evaluation

For histological staining, the excised tibial specimens were fixed in 4% paraformaldehyde, decalcified in EDTA, dehydrated in a graded series of ethanol solutions, and embedded in paraffin. HE staining was then conducted to observe tissue morphology as well as cell survival and death. Masson staining was performed to observe the distributions of collagen and muscle fibers. Toluidine blue staining was performed to

observe the morphology of cartilage and the number and distribution of mast cells. The following criteria were used for histological assessment of bone infection: abscess formation with edema in the intramedullary canal or cortical bone, infiltration of inflammatory cells (neutrophil granulocytes, lymphocytes, plasma cells, and multinuclear giant cells), detection of bacteria, destruction of the lamellar bone structure with subperiosteal bone formation, lifting of the periosteum, formation of bone necrosis with empty osteocyte lacunae, and/or formation of bone sequestrs.

Immunohistochemical staining

For histological staining, excised tibial specimens were fixed in 4% paraformaldehyde, decalcified in EDTA, dehydrated in a graded series of ethanol solutions, and embedded in paraffin. Sagittal sections of specimens were incubated with primary antibodies against ALP (bs-6292r, 1:300), OCN (bs-4917r, 1:300), and OPN (bs-0026r, 1:300). Secondary antibodies were applied for 1 h at room temperature. The numbers of ALP-positive cells (N.ALP+), OCN-positive cells (N.OCN+) and OPN-positive cells (N.OPN+) around the bone defect area were calculated and analyzed quantitatively (Olympus BX63).

Proteomics analysis

Proteomics analysis mainly included protein extraction, peptide enzymatic hydrolysis, TMT labeling, chromatographic grading, LC-MS/MS data collection, protein identification and quantitative analysis, screening of differentially expressed proteins, and analysis of differentially expressed protein clustering. A detailed description can be found in the online supplementary text and elsewhere [19].

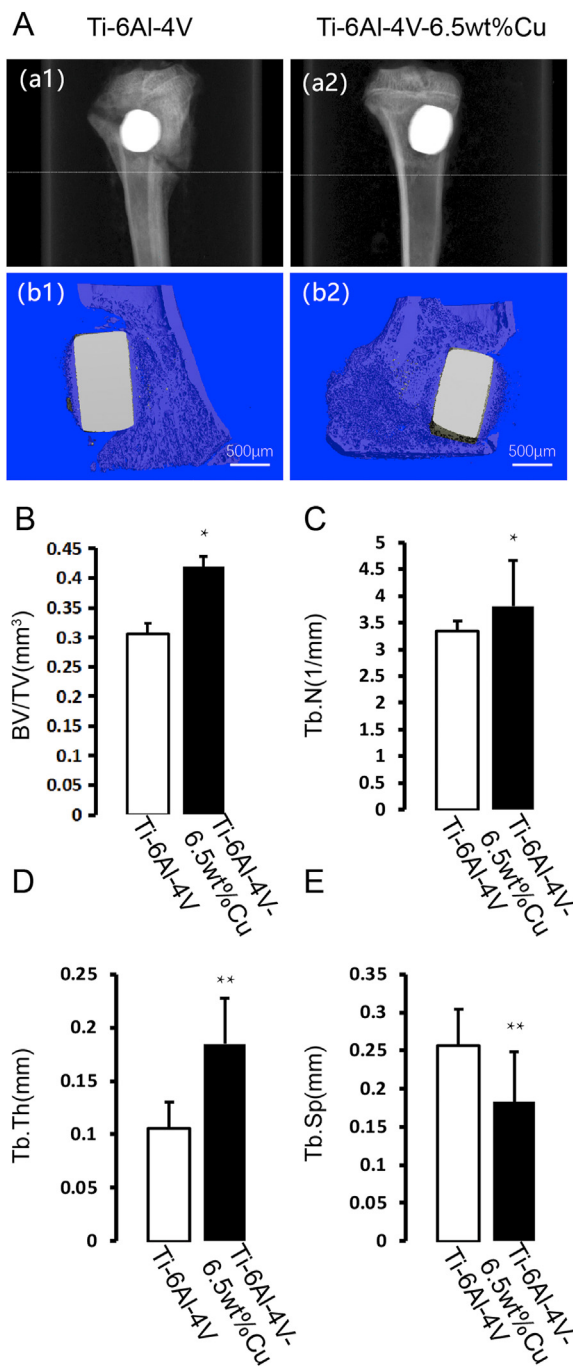


Fig. 5. A(a1) X-ray imaging of Ti6Al4V alloy. A(a2) X-ray imaging of Ti6Al4V-6.5wt%Cu alloy. A(b1) Three-dimensional μ CT images of Ti6Al4V alloy. A(b2) Three-dimensional μ CT images of Ti6Al4V-6.5wt%Cu alloy. (B) Quantitative micro-CT analysis of the tibial bone around an implant: BV/TV, (C) number of Tb.N, (D) Tb.Th, and (E) Tb.Sp. A = Bone defect implanted with B (allow). B = Bone defect implanted with A (allow). n = 5 per group. *p < 0.05 compared with group A, **p < 0.01 compared with group A.

Protein digestion and iTRAQ labeling

Protein digestion was performed according to the FASP procedure described by Wisniewski, Zougman et al. (2009) [19] and the resulting peptide mixture was labeled using the 4-plex/8-plex iTRAQ reagent according to the manufacturer's instructions (Applied Biosystems). Briefly, 200 μ g of proteins for each sample were incorporated into 30 μ l STD buffer (4% SDS, 100 mM DTT, 150 mM Tris-HCl pH 8.0). The detergent, DTT and other low-molecular-weight components were removed using

UA buffer (8 M Urea, 150 mM Tris-HCl pH 8.0) by repeated ultrafiltration (Microcon units, 30 kD). Then 100 μ l 0.05 M iodoacetamide in UA buffer was added to block reduced cysteine residues and the samples were incubated for 20 min in darkness. The filters were washed with 100 μ l UA buffer three times and then 100 μ l DS buffer (50 mM triethylammoniumbicarbonate at pH 8.5) twice. Finally, the protein suspensions were digested with 2 μ g trypsin (Promega) in 40 μ l DS buffer overnight at 37°C, and the resulting peptides were collected as a filtrate. The peptide content was estimated by UV light spectral density at 280 nm using an extinction coefficient of 1.1 of 0.1% (g/L) solution that was calculated on the basis of the frequency of tryptophan and tyrosine in vertebrate proteins.

For labeling, each iTRAQ reagent was dissolved in 70 μ l of ethanol and added to the respective peptide mixture. The samples were labeled as (Sample1)-114, (Sample2)-115, (Sample3)-116, and (Sample4)-117, and were multiplexed and vacuum dried.

Peptide fractionation with strong cation exchange (SCX) chromatography

iTRAQ labeled peptides were fractionated by SCX chromatography using the AKTA purifier system (GE Healthcare). The dried peptide mixture was reconstituted and acidified with 2 ml buffer A (10 mM KH₂PO₄ in 25% of ACN, pH 2.7) and loaded onto a PolySULFOETHYL 4.6 \times 100 mm column (5 μ m, 200 Å, PolyLC Inc, Maryland, U.S.A.). The peptides were eluted at a flow rate of 1 ml/min with a gradient of 0%–10% buffer B (500 mM KCl, 10 mM KH₂PO₄ in 25% of ACN, pH 2.7) for 2 min, 10–20% buffer B for 25 min, 20%–45% buffer B for 5 min, and 50%–100% buffer B for 5 min. The elution was monitored by absorbance at 214 nm, and fractions were collected every 1 min. The collected fractions (about 30 fractions) were finally combined into 10 pools and desalted on C18 Cartridges (Empore™ SPE Cartridges C18 (standard density), bed I.D. 7 mm, volume 3 ml, Sigma). Each fraction was concentrated by vacuum centrifugation and reconstituted in 40 μ l of 0.1% (v/v) trifluoroacetic acid. All samples were stored at –80°C until LC-MS/MS analysis.

Liquid chromatography (LC) – electrospray ionization (ESI) tandem MS (MS/MS) analysis by Q Exactive

Experiments were performed on a Q Exactive mass spectrometer that was coupled to Easy nLC (Proxeon Biosystems, now Thermo Fisher Scientific). 10 μ l of each fraction was injected for nano LC-MS/MS analysis. The peptide mixture (5 μ g) was loaded onto a C18-reversed phase column (Thermo Scientific Easy Column, 10 cm long, 75 μ m inner diameter, 3 μ m resin) in buffer A (0.1% Formic acid) and separated with a linear gradient of buffer B (80% acetonitrile and 0.1% Formic acid) at a flow rate of 250 nl/min controlled by IntelliFlow technology over 140 min. MS data were acquired using a data-dependent top10 method to dynamically choose the most abundant precursor ions from the survey scan (300–1800 m/z) for HCD fragmentation. Determination of the target value was based on predictive Automatic Gain Control (pAGC). Dynamic exclusion duration was 60 s. Survey scans were acquired at a resolution of 70,000 at m/z 200 and resolution for HCD spectra was set to 17,500 at m/z 200. Normalized collision energy was 30 eV and the underfill ratio, which specifies the minimum percentage of the target value likely to be reached at maximum fill time, was defined as 0.1%. The instrument was run with peptide recognition mode enabled.

Sequence database searching and data analysis

We searched the Uniprot Human database (<https://www.uniprot.org/>) using the keywords “osteogenic differentiation, osteoblast, ossification, and bone mesenchymal stem cell” to identify proteins that were clearly related to osteogenic differentiation in humans. In the same manner, we used “bone calcification, bone matrix mineralization, and bone mineralization” as keywords to identify proteins associated with bone mineralization. The online tool STRING database (<http://www.string-db.org/>) was used to establish the protein-to-protein

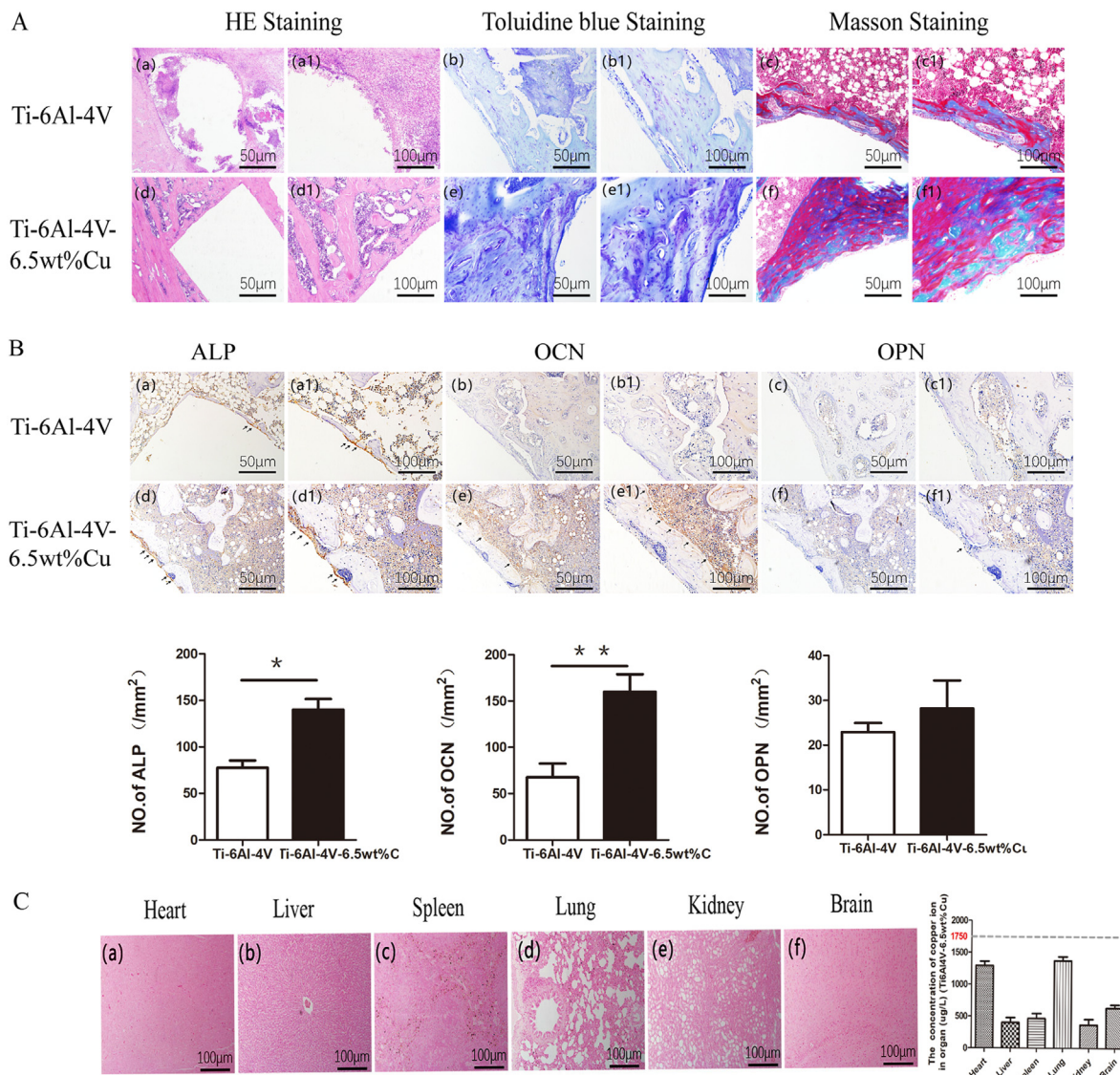


Fig. 6. (A) HE staining [(a) and (a1)], Toluidine blue staining [(b) and (b1)] and Masson staining [(c) and (c1)] of Ti6Al4V alloy; HE staining [(d) and (d1)], Toluidine blue staining [(e) and (e1)] and Masson staining [(f) and (f1)] of Ti6Al4V-6.5wt%Cu alloy. (B) Immunohistochemical staining of ALP [(a) and (a1)], OCN [(b) and (b1)], and OPN [(c) and (c1)] in the Ti6Al4V alloy group; immunohistochemical staining of ALP [(d) and (d1)], OCN [(e) and (e1)], and OPN [(f) and (f1)] in the Ti6Al4V-6.5wt%Cu alloy group. (C) Copper salt staining of heart (a), liver (b), spleen (c), lung (d), kidney (e) and brain (f) in the Ti6Al4V-6.5wt%Cu alloy group.

Table 2

Protein identification results.

Database	Spectra [PSM]	Peptides	Unique	Protein groups
<i>Rattus norvegicus</i> . Rnor	96,315	30,037	25,338	4279

interacting (PPI) network between the DEPs and osteogenesis or bone mineralization-related proteins searched for above to identify the key DEPs (Szkłarczyk and Jensen 2015). We screened out DEPs homologous in humans and rats, which interacted with osteogenesis and bone mineralization-related proteins. Cytoscape software version 3.7.1 was used to analyze the degree of distribution, closeness centrality, and betweenness centrality. Nodes with more edges (interactions) among the various nodes (proteins) were identified as key proteins that played a major role in the PPI network. All DEPs with a high degree of relatedness were selected.

Statistical analysis

Data were presented as the means ± standard deviations of at least three independent measurements of each sample (each group included at least six statistically valid samples). One-way analysis of variance (ANOVA) was used for multifactorial comparisons. Specifically, if no heterogeneity was observed, the Bonferroni test was used to assess the differences between groups. If heterogeneity did exist, the Welch test was used to test the equality of means and the Dunnett’s T3 test was used to assess the differences between groups. All data analyses were conducted with SPSS 22.0 analysis software (SPSS Inc). Differences were considered significant at *p < 0.05 or **p < 0.01.

Results

In vitro assessment of antibacterial activity

Biofilm formation

Ti6Al4V alloy material was co-cultured with 1 × 10⁵ cfu/ml *S. aureus*

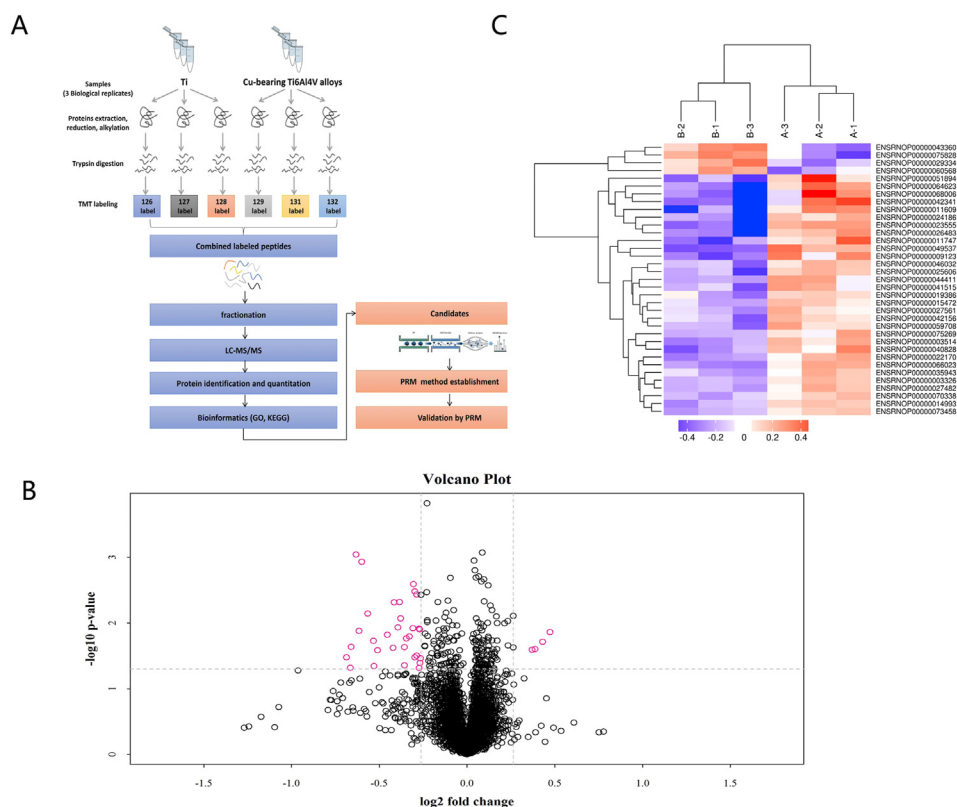


Fig. 7. (A) Flow chart showing proteomics analysis, including proteome extraction, peptidase hydrolysis, TMT labeling, chromatography classification, LC-MS/MS data collection, protein identification and quantitative analysis, differential protein screening, and differential expression protein cluster analysis. (B) The volcano plot was drawn using two factors, difference in protein expression between two sample sets and p-value obtained by the t-test, to show significant differences between two sets of sample data. The abscissa indicates the difference of the multiplier (base 2 logarithmic change), and the ordinate the difference of the p-value (base 10 logarithmic transformation). Red points in the figure indicate significantly differentially expressed proteins (fold change greater than 1.2 times and $p < 0.05$), and black spots proteins with no significantly different expression. (C) Results of the cluster analysis were represented by a tree-shaped heatmap in which each row represents a protein (whose ordinate is significantly differentially expressed), and each column a group of specimens (the abscissa is the specimen information). Red represents a significantly upregulated protein, blue a significantly downregulated protein, and gray a protein with no quantitative information.

for 3, 6, 12, 24, 48 and 96 h. Biofilm formation by bacteria on the edge of the material was observed after 3 h, but the area with relatively smooth polishing in the center of the material had no obvious bacteria because the bacteria did not colonize easily (Figs. 2 a-1). At 6 h of biofilm adhesion, the central region of biofilm on the adhesive material distributed irregularly at the edges (Figs. 2 b-1). The biofilm at 12 h was concentrated on the material surface (Figs. 2 c-1). At 24 h and 48 h when the mature phase of the biofilm was reached, a fluorescent white film distributed on the surface of the material (Figs. 2 d-1, e-1). At 96 h, the biofilm matured further, and the enhanced fluorescent white film widely distributed on the material surface (Figs. 2 f-1).

Ti6Al4V-6.5wt%Cu alloy was also co-cultured with 1×10^5 cfu/ml *S. aureus* for 3, 6, 12, 24, 48 and 96 h. Neither bacterial colonization at the edge or center of the material nor biofilm formation was observed at 3 h (Fig. 2 a-2). At 6 h, a small amount of biofilm formed and attached to the edge of the material (Fig. 2 b-2). At 12 h and 24 h, biofilm formation increased but was still mainly in the adhesion stage (Fig. 2 c-2 and d-2). At 48 h, maturation of copper ions or aging of the biofilm was observed, and the fluorescent biofilm increased (Fig. 2e-2). The fluorescence of biofilm decreased gradually after 48 h, indicating the aging stage. At 96 h, we observed obviously decreased bacterial biofilm in Ti-6Al-4V-6.5wt %Cu group (Fig. 2 f-2). The bacterial biofilm in Ti-6Al-4V-6.5wt%Cu group at each time point was significantly less than in Ti-6Al-4V group.

Detection of dead and live bacteria by confocal laser scanning microscopy

After co-cultured with pathogenic *S. aureus* for 3 h, Ti6Al4V-6.5wt% Cu alloy showed less adherence of active *S. aureus* than Ti6Al4V alloy [Fig. 3A(a-1) and (a-2)]. After co-culture for 6 h, the percentage of viable *S. aureus* on Ti6Al4V-6.5wt%Cu alloy began to decline [Fig. 3A(b-1) and (b-2)], and the percentage of viable *S. aureus* on Ti6Al4V-6.5wt%Cu alloy was less than 40% after co-culture for 8 h [Fig. 3A(c-1) and (c-2)]. The percentage of viable *S. aureus* on Ti6Al4V alloy showed an increasing trend but the percentage of viable bacteria remained at 55%–90% after co-culture for 12 h [Fig. 3A(d-1) and (d-2)]. After 24 h of co-culture, the percentage of viable bacteria in the two groups began to decrease

[Fig. 3A(e-1) and (e-2)]. After 48 h of culture, the percentage of viable bacteria in the two groups decreased by 50% or less [Fig. 3A(f-1) and (f-2)]. Therefore, during the co-culture period of 3–6 h, the live rate of *S. aureus* in the Ti6Al4V-6.5wt%Cu alloy showed a trend of decreasing (Fig. 3B), indicating Ti6Al4V-6.5wt%Cu alloy inhibited the activity of *S. aureus* at the early stage of bacterial adhesion and accelerated its aging and death at 6–8 h. The percentage of dead bacteria in the Ti6Al4V-6.5wt %Cu alloy increased continuously during co-culture for 6–8 h (Fig. 3C), suggesting that Ti6Al4V-6.5wt%Cu alloy inhibited the activity of *S. aureus* at the early stage of bacterial adhesion for 6–8 h. In short, in the control group, the percentage of dead bacteria decreased significantly after 6–12 h of co-culture. After co-culture for 8–24 h, the percentage of dead *S. aureus* in the experimental group was lower than 50%. After co-culture with *S. aureus* for 24 h, the percentage of dead bacteria in the experimental group was up to 40% but only 20% in the control group. These results suggested that the Ti6Al4V-6.5wt%Cu alloy had an obvious antibacterial effect, inhibiting the activity of *S. aureus* at an early stage and accelerating its aging and death at 6–8 h.

In vivo assessment of antibacterial activity

General observations and laboratory test indexes

Signs of soft tissue infection in lower limbs like leg swelling, skin ulcer, pus formation and yellow fluid exudation in the control group [Fig. 4A(c)] were more serious than in the experimental group [Fig. 4A(e)]. The tibial bone tissue in the control group was obviously swollen and the volume of the medullary cavity was enlarged [Fig. 4A(d)]. Bone tissue destruction in the experimental group [Fig. 4A(f)] was no more serious than in the control group [Fig. 4A(d)]. The local skin temperature in the control group was significantly higher than in the experimental group and sham group. The local skin temperatures in both groups reached the peak on day 3 and then decreased gradually. The local skin temperature in the control group was higher than in the experimental group (Fig. 4B). White blood cells and neutrophils in both groups were increased significantly compared with the sham group.

Table 3
Differentially expressed proteins identified by comparison.

Accession	protein_name	gene_name	Coverage	B/A	p value
ENSRNOP00000075828	serine and arginine rich splicing factor 3	Srsf3	16.13	1.39	0.01
ENSRNOP00000043360	—	AABR07061152.1	2.81	1.35	0.02
ENSRNOP00000029334	dihydropyrimidinase-like 4	Dpysl4	2.80	1.31	0.02
ENSRNOP00000060568	ribosomal protein S28	Rps28	46.38	1.29	0.03
ENSRNOP00000027561	syntrophin, beta 2	Sntb2	4.41	0.83	0.03
ENSRNOP00000075269	tubulin, beta 5 class I	Tubb5	68.24	0.83	0.04
ENSRNOP00000070338	testin LIM domain protein	Tes	5.01	0.83	0.01
ENSRNOP00000015472	cyclin D1 binding protein 1	Ccnbdp1	3.34	0.83	0.01
ENSRNOP00000019386	syndecan 4	Sdc4	11.88	0.83	0.05
ENSRNOP00000035943	CCR4-NOT transcription complex, subunit 11	Cnot11	2.38	0.82	0.03
ENSRNOP00000073458	NmrA like redox sensor 1	Nmr1	20.07	0.82	0.00
ENSRNOP00000042156	Ttk protein kinase	Ttk	1.56	0.81	0.03
ENSRNOP00000003326	hematopoietic cell specific Lyn substrate 1	Hcls1	7.77	0.81	0.00
ENSRNOP00000014993	SS nuclear autoantigen 1	Ssna1	9.24	0.81	0.00
ENSRNOP00000027482	TATA-box binding protein associated factor 5	Taf5	1.75	0.81	0.01
ENSRNOP00000046032	DAZ associated protein 1	Dazap1	10.37	0.80	0.02
ENSRNOP00000059708	hypothetical protein LOC100359583	LOC100359583	25.89	0.79	0.02
ENSRNOP00000044411	glutamic-pyruvic transaminase	Gpt	1.81	0.78	0.02
ENSRNOP00000041515	—	AC128207.1	12.56	0.78	0.04
ENSRNOP00000022170	nuclear autoantigenic sperm protein	Nasp	11.21	0.77	0.01
ENSRNOP00000003514	calcium regulated heat stable protein 1	Carhsp1	10.88	0.77	0.00
ENSRNOP00000025606	troponin C1, slow skeletal and cardiac type	Tnnc1	6.83	0.76	0.01
ENSRNOP00000066023	KH-type splicing regulatory protein	Khsrp	36.06	0.75	0.00
ENSRNOP00000040828	agrin	Agri	1.80	0.75	0.02
ENSRNOP00000024186	myosin heavy chain 7	Myh7	39.33	0.73	0.01
ENSRNOP00000011747	angiotensin II receptor-associated protein	Agtrp	4.38	0.70	0.03
ENSRNOP00000051894	sialophorin	Spn	15.05	0.69	0.05
ENSRNOP00000009123	A-kinase anchoring protein 14	Akap14	1.39	0.69	0.02
ENSRNOP00000026483	A-kinase anchoring protein 12	Akap12	6.13	0.68	0.01
ENSRNOP00000049537	glycophorin C (Gerbich blood group)	Gypc	27.37	0.66	0.00
ENSRNOP00000011609	U2 snRNP-associated SURP domain containing	U2surp	2.44	0.65	0.01
ENSRNOP00000023555	apolipoprotein B receptor	Apob	1.78	0.64	0.00
ENSRNOP00000064623	high mobility group nucleosome binding domain 5	Hmgn5	2.99	0.63	0.02
ENSRNOP00000068006	stathmin 1	Stmn1	40.27	0.63	0.05
ENSRNOP00000042341	hemogen	Hemgn	12.65	0.62	0.03

salt staining showed no copper ion deposition in heart [Fig. 6C(a)], liver [Fig. 6C(b)], spleen [Fig. 6C(c)], lung [Fig. 6C(d)], kidney [Fig. 6C(e)] or brain [Fig. 6C(f)] in the experimental group, indicating no effect of copper ions on animal organs. In short, these results demonstrated that Ti6Al4V-6.5wt%Cu alloy reduced inflammation and enhanced osteogenesis and biosafety.

Proteomics

Protein identification and differential protein expression (DEPs)

A total of 4279 proteins were identified in rats by TMT quantitative proteomics (Table 2). The detailed information is shown in Supplementary materials. DEPs were screened according to the standard of the expression multiple with changes of >1.2 times (increased by > 1.2 times or decreased by < 0.83 times) and a p-value of <0.05. The number of DEPs was determined in each comparison group. Quantitative statistical results of proteins were presented in the form of a volcano plot (Fig. 7B). Among them, there were four upregulated DEPs and 31 downregulated DEPs in the experimental group versus the control group.

Cluster analysis of differentially expressed proteins

Cluster analysis was used to analyze DEPs in the comparison group, and the data were presented in the form of heat map. The results of cluster analysis were represented by a tree shaped heat map, in which each row represented a kind of protein (the vertical coordinate represented a significantly different protein), and each column represented a group of samples (the horizontal coordinate was the sample information). Red represented a significantly up-regulated protein, blue a significantly down regulated protein, and grey no quantitative protein information (Fig. 7C). DEPs were screened according to the Student’s t-test and one-way ANOVA of the expression multiple with changes of >1.2 times and a p-value of <0.05.

Table 4
Target proteins associated with osteogenic differentiation.

Degree	Betweenness Centrality	Closeness Centrality	Gene name
27	0.009972	0.450139	SDC4
21	0.012811	0.442177	AGRN
11	0.00155	0.393939	KHSRP
11	0.000772	0.357143	SRSF3
10	0.010793	0.363128	MYH7
9	0.000392	0.396341	AKAP12
8	0.000247	0.417202	GPT
8	0.007414	0.376593	TTK
8	0.001126	0.331971	U2SURP
7	0.00164	0.406758	STMN1
6	0.0000779	0.399263	SPN
6	0.006212	0.316148	RPS28
6	0	0.378347	AGTRAP
5	0.000308	0.308349	DAZAP1
5	0.000302	0.317383	NASP
4	0.0000114	0.373993	HCLS1
3	0.000778	0.378788	CARHSP1
3	0.000722	0.309524	TES
3	0.000109	0.288889	TNNC1
2	0.000228	0.377907	HMGN5
2	0.0000119	0.318627	HEMGN
2	0.000147	0.27403	SSNA1
1	0	0.308935	CCNDBP1
1	0	0.376593	GYPC
1	0	0.281873	CNOT11

GO function analysis

The results based on the second level showed that DEPs in the experimental group versus the control group in the comparison group were mainly involved in cellular process, metabolic process, response to stimulus, cellular component organization or biogenesis and

Table 5
Target proteins associated with cellular mineralization.

Degree	Betweenness Centrality	Closeness Centrality	Gene Name
5	0.001932	0.368852	SDC4
5	0.002179	0.378151	AGRN
4	0.001284	0.368852	GPT
3	0.022655	0.314685	MYH7
2	0.5	0.571429	DAZAP1
2	0.001203	0.301003	NASP
2	0.002436	0.315789	TTK
2	0.000661	0.289389	AKAP12
2	0.666667	0.666667	STMN1
2	0.666667	0.666667	KHSRP
2	0.5	0.571429	SRSF3
1	0	0.4	CARHSP1
1	0	0.224439	RPS28
1	0	0.299003	HCLS1
1	0	1	AKAP14
1	0	0.283912	HEMGN
1	0	0.24	TNNC1
1	0	0.4	SSNA1
1	0	0.4	TAF5
1	0	0.290323	AGTRAP
1	0	0.4	U2SURP

multicellular organismal process, and other important biological processes, and they distributed mainly in the cell, cell part, organelle, organelle part and membrane with binding, catalytic activity, and structural molecular activity. There were more DEPs in the biological progress.

Biological pathway analysis

KEGG pathway analysis showed that the DEPs in the experimental group versus the control group were mainly involved in the Epstein-Barr virus infection pathway, ECM-receptor interaction pathway, and Herpes simplex infection pathway (Fig. 8B).

Two differential regulated proteins were included in the Epstein-Barr virus infection pathway. Both of them were down-regulated in the experimental group: hypothetical protein LOC100359583 (FC = 0.786) and sialoporphin (FC = 0.692). Syndecan 4 (FC = 0.827) and agrin (FC = 0.746) were down-regulated and involved in the ECM-receptor interaction pathway. For differentially regulated proteins involved in the Herpes simplex infection pathway, serine and arginine rich splicing factor 3 was up-regulated with a FC of 1.388 while TATA-box binding protein associated factor 5 was down-regulated with a FC of 0.807.

Protein-protein interaction network analysis (PPI)

To further explore the mechanism of osteogenic mineralization in Ti6Al4V-6.5wt%Cu alloy, we conducted protein-protein interaction (PPI) network analysis of the DEPs, osteogenesis and bone calcification-associated proteins as well (Fig. 8C, Table 3). The nodes represent the proteins in the PPI network and the lines the interaction among the proteins. Fig. 8C showed PPI network of osteogenesis-associated and bone mineralization-related proteins and DEPs. The size and color of nodes are associated with the significance of proteins while the thickness of lines is proportional to the strength of interactions among proteins. The results showed that there were 328 nodes and 3713 edges in the osteogenesis-associated PPI network and there were 105 nodes and 367 edges in the bone calcification-associated PPI network (Fig. 8C). SDC4 and AGRN degrees were the highest among the proteins that interacted with osteogenesis-related proteins and mineralization-related proteins, which may indicate that these genes play a role in bone cell differentiation and bone mineralization. Target proteins associated with osteogenic differentiation (Table 4). Target proteins associated with cellular mineralization (Table 5).

Discussion

In this study, we demonstrated the antimicrobial and bone-promoting effects of the antimicrobial material, Ti6Al4V-6.5wt%Cu alloy, and its related mechanisms *in vivo*.

Ti6Al4V-6.5wt%Cu alloy is composed of three phases of alpha, beta, and Ti₂Cu. It has been shown that, in present processing of Ti6Al4V-6.5wt%Cu alloy, air cooling annealing at 740° has led to the best antimicrobial effect and a strong killing effect on *S. aureus* and *Escherichia coli* [15]. A preliminary analysis of the antimicrobial mechanism has indicated that adding an appropriate amount of antimicrobial Cu ions to the Ti matrix releases copper ions and a combination of positive charge of copper ions with bacteria has a bactericidal function [15]. When titanium alloy containing copper ions is implanted into a human body, it has a sustained antimicrobial effect, thereby reducing or inhibiting infection after implantation [21]. Furthermore, release of copper ions does not damage the body. We found that the antimicrobial metallic material inhibited or delayed formation of bacterial biofilm of pathogenic *S. aureus in vitro*, thus preventing infection after internal fixation and improving efficacy of antibacterial treatment. Consistently, our present study demonstrated that Ti6Al4V-6.5wt%Cu alloy has good mechanical properties, malleable plasticity, and good biological safety.

We successfully established animal models of a single infected bone defect in SD rats to test the antibacterial effect of Ti6Al4V-6.5wt%Cu alloy. A bone defect with φ3 mm in diameter is not large enough to meet the experimental needs over 6 weeks because the defect may heal ahead of the due time while a φ5-mm bone defect is too large because it increases the risk of bone fracture [22,23]. This study, therefore, decided the critical diameter of the proximal tibial bone defect to be 4 mm. Because *S. aureus* is the most common pathogen for infection after orthopedic internal fixation [2], it was used in this study at 1 × 10⁵ cfu/ml. Our establishment of animal models was confirmed by clinical manifestations, laboratory examinations of blood indicators, imaging analysis, and histomorphological evaluation, demonstrating that our models of infected bone defect in SD rats were reliable simulation of infected bone nonunion and other complications.

We investigated whether Ti6Al4V-6.5wt%Cu alloy could effectively inhibit or delay bone infection after it had been implanted into the infected bone defect. When used as an implant material, it should have an antimicrobial function to prolong the wound debridement time for patients with early infection or suspected infection after internal fixation. We took Ti6Al4V alloy as a control to observe the time-effect relationship during the process of adhesion, aggregation, extension and aging of pathogenic *S. aureus* on the metal surface. Compared with Ti6Al4V alloy, the time for biofilm adhesion onto the surface of Ti6Al4V-6.5wt%Cu alloy was longer. On Ti6Al4V alloy, pathogenic *S. aureus* began to form biofilm adhesion and aggregation after coculture for 3 h and tended to mature after 24 h. However, the biofilm adherence of pathogenic *S. aureus* onto Ti6Al4V-6.5wt%Cu alloy did not occur until 6 h after coculture and the biofilm on the metal surface tended to age after 24 h. The above phenomena indicated that Ti6Al4V-6.5wt%Cu alloy obviously suppressed formation of bacterial biofilm and accelerated biofilm aging or death. Laser scanning confocal microscopy showed that the percentage of viable bacteria adhering onto Ti6Al4V alloy surface was 55%–90% while that onto Ti6Al4V-6.5wt%Cu alloy surface less than 40%. Obviously, Ti6Al4V-6.5wt%Cu alloy had an obvious bacteriostatic activity at the early stage of bacterial adhesion. A previous study shows that Cu-bearing titanium with an antimicrobial activity inhibits biofilm by releasing Cu ions from its surface [24]. It is crucial to efficiently kill bacteria and discourage biofilm formation on implant surfaces to inhibit bacterial infection and prevent implantation failure. Ti6Al4V-6.5wt%Cu alloy showed an excellent antimicrobial activity and inhibited biofilm formation *in vitro* [14], but further study is required to clarify whether the *in vivo* antibacterial effect of this material is effective. Therefore, we implanted Ti6Al4V-6.5wt%Cu alloy into bone defects *in vivo*. Results showed that animals implanted with 6.5wt.% Cu alloy exhibited a lower

local skin temperature, milder inflammatory exudation and local ulceration, unobvious tibial swelling, slightly swollen medullary cavity, and faster wound healing than those implanted with Ti6Al4V alloy and that their body temperature, and C-reactive protein and leucocyte levels were also significantly lower. These suggested that Ti6Al4V-6.5wt%Cu alloy significantly reduced the inflammatory reaction after infection and its anti-bacterial effect *in vivo* might have been associated with its inhibition of biofilm formation *in vitro*.

We next determined whether Ti6Al4V-6.5wt%Cu alloy promoted osteogenesis or induced bone regeneration *in vivo*. Our results showed that Ti6Al4V-6.5wt%Cu alloy prevented infection and promoted regeneration of new bone tissue in the infected bone defect area. A previous study shows that copper-loaded chitosan scaffolds improve bone regeneration of skull defects critically sized in rats by releasing copper ions [25]. Our study revealed that new bone was bound to Ti6Al4V-6.5wt%Cu alloy more tightly than to Ti6Al4V alloy, indicating that Ti6Al4V-6.5wt%Cu alloy has better biocompatibility. Studies have shown that copper ions significantly promote osteogenic differentiation of hBMSCs by improving expression of bone-related genes like alkaline phosphatase (ALP), osteopontin (OPN), and osteocalcin (OCN) [26–28]. Our immunohistochemical staining showed that the expression of osteogenic proteins in bone tissue around the infected bone defects filled with Ti6Al4V-6.5wt%Cu alloy was significantly higher than that filled with Ti6Al4V alloy. Ti6Al4V-6.5wt%Cu alloy promoted repair of local bone defects by releasing copper ions and increasing new bone formation to promote bone healing while it resisted infection.

Previous studies have shown that Ti–Cu alloy materials have good biocompatibility and promote osteogenesis, but the related proteins are still unclear. To further investigate the osteogenesis of Ti6Al4V-6.5wt%Cu alloy, we first used ITRAQ-based proteomics to obtain protein profiles. The results showed that Ti6Al4V-6.5wt%Cu alloy affected important biological processes such as cell process, metabolic process, stimulus response, cell constituent tissue or biogenesis, and multicellular biological process. We identified 35 differently expressed proteins. One of the obvious characteristics was that more proteins were down-regulated than up-regulated in bone tissue, indicating that Ti6Al4V-6.5wt%Cu alloy might perform antibacterial function and promote osteogenesis by down-regulating proteins related to bone tissue. To further explore the mechanism of osteogenic mineralization of Ti6Al4V-6.5wt%Cu alloy, we screened for differential genes with osteogenic and mineralized proteins, and screened out the differential genes that interacted with these proteins. The results showed that SDC4 and AGRN were the top two target proteins associated with osteogenic differentiation and bone mineralization. A previous study shows that SDC4 is overexpressed in OA cartilage. SDC4, encoding syndecan-4, is a positive regulator of articular cartilage breakdown. As Borland et al. reported that SDC4 inhibited mineral deposition, our study also found that Ti6Al4V-6.5wt%Cu alloy downregulated the expression of SDC4. Therefore, it is reasonable to speculate that Ti6Al4V-6.5wt%Cu alloy may promote bone formation by inhibiting the expression of SDC4, which may suppress cartilaginous callus formation and mineralization [29]. Agrin may inhibit expression of BMP2 and BMP4. Since BMP-2 is a key protein in bone formation, Ti6Al4V-6.5wt%Cu alloy may inhibit expression of agrin protein to stimulate expression of BMP-2 and promote bone formation [30]. Studies have shown that SDC4 knockdown in alveolar epithelial cells or blocking it with anti-SDC4 antibody can reduce mycobacterial attachment and internalization [31]. In addition, highly pathogenic *H. pylori* strains induce SDC4 expression, in both human gastric mucosa and gastric cell lines, in a cagPAI-dependent manner [32]. AGRN is closely linked to immunity. Previous studies show that agrin has been detected in lymphocytes and down-regulation of its expression leads to inhibition of both antigen-specific and nonspecific lymphocyte activation [33]. Now, AGRN is believed to act as a bridge between the nervous and immune systems [34]. All these suggest that AGRN plays an important role in immune regulation. Therefore, although no studies have shown the direct relationship between SDC4/AGRN and *S. aureus*, it is reasonable to assume

that SDC4/AGRN is responsible for infection and inflammation. The specific signaling mechanism of SDC4/AGRN for osteogenesis and infection calls for further study.

In conclusion, the present study demonstrates that Ti6Al4V-6.5wt%Cu alloy has good antibacterial and osteogenic effects *in vivo* and *in vitro*. We have shown for the first time that SDC4 and AGRN may be involved in the antibacterial and osteogenesis effects of Ti6Al4V-6.5wt%Cu alloy *in vivo*. The osteogenesis of Ti6Al4V-6.5 wt%Cu Alloy may promote the osteogenic differentiation of pre-osteoblasts and bone marrow mesenchymal stem cells by down-regulating SDC4 and Agrin. Therefore, further studies are needed to clarify the role of these proteins in bone infection and the specific mechanism of the signaling pathway.

Funding

The study was supported by the Medical Technique and Research Program of Guangdong Province, China (grant number A2017463); China Postdoctoral Science Foundation, China (grant number 2017M613432); Youth Training Program for Military Medical Science and Technology (grant number 19QNP005) and Guangdong Medical Science And Technology Research Foundation (grant number 2016102511210492).

This work was financially supported by the National Key Research and Development Program of China (NO.2018YFC1106601) and Promoting Liaoning Province Talents Program – Top Young Talents (XLYC1807069).

Conflict of Interest

The authors have no conflicts of interest to disclose in relation to this article.

Acknowledgment

Bin Yu, Ling Ren and Hong Xia conceived and designed the experiments. Jun Yang and Hanjun Qin performed the experiments. Jun Yang, Hanjun Qin and Yu Chai wrote the manuscript. Ping Zhang, Ke Yang, Min Qin and Yirong Chen analyzed the data and prepared all the figures. Yifang Zhang revised and edited the final manuscript in both language and organization. All authors reviewed and agreed upon the final manuscript. We thank Liwen Bianji, Edanz Group China (www.liwenbianji.cn/ac) for editing an English draft of this manuscript.

Appendix A. Supplementary data

Supplementary data to this article can be found online at <https://doi.org/10.1016/j.jot.2020.10.004>.

References

- [1] Katsikogianni M, Missirlis YF. Concise review of mechanisms of bacterial adhesion to biomaterials and of techniques used in estimating bacteria-material interactions. *Eur Cell Mater* 2004;8:37–57.
- [2] Riool M, de Boer L, Jaspers V, van der Loos CM, van Wamel WJB, Wu G, et al. Staphylococcus epidermidis originating from titanium implants infects surrounding tissue and immune cells. *Acta Biomater* 2014;10:5202–12.
- [3] Junter G, Thébault P, Lebrun L. Polysaccharide-based antibiofilm surfaces. *Acta Biomater* 2016;30:13–25.
- [4] Tuson HH, Weibel DB. Bacteria-surface interactions. *Soft Matter* 2013;9:4368–80.
- [5] Nukavarapu SP, Dorcenus DL. Osteochondral tissue engineering: current strategies and challenges. *Biotechnol Adv* 2013;31:706–21.
- [6] Geetha M, Singh AK, Asokamani R, Gogia AK. Ti based biomaterials, the ultimate choice for orthopaedic implants – a review. *Prog Mater Sci* 2009;54:397–425.
- [7] Carson JS, Bostrom MP. Synthetic bone scaffolds and fracture repair. *Injury* 2007; 38(Suppl 1):S33–7.
- [8] Dehghanghadikolaei A, Fotovvati B. Coating techniques for functional enhancement of metal implants for bone replacement: a review. *Materials* 2019;12 (Basel).
- [9] Ahmadiadegan H, Esmailzadeh S, Ranjbar M, Marzban Z, Ghavas F. Synthesis and characterization of polyester bionanocomposite membrane with ultrasonic irradiation process for gas permeation and antibacterial activity. *Ultrason Sonochem* 2018;41:538–50.

- [10] Fan Z, Qin Y, Liu S, Xing R, Yu H, Chen X, et al. Synthesis, characterization, and antifungal evaluation of diethoxyphosphoryl polyaminoethyl chitosan derivatives. *Carbohydr Polym* 2018;190:1–11.
- [11] Godoy-Gallardo M, Manzanares-Céspedes MC, Sevilla P, Nart J, Manzanares N, Manero JM, et al. Evaluation of bone loss in antibacterial coated dental implants: an experimental study in dogs. *Mater Sci Eng C* 2016;69:538–45.
- [12] Li Y, Liu L, Wan P, Zhai Z, Mao Z, Ouyang Z, et al. Biodegradable Mg-Cu alloy implants with antibacterial activity for the treatment of osteomyelitis: in vitro and in vivo evaluations. *Biomaterials* 2016;106:250–63.
- [13] Ren X, Yang C, Zhang L, Li S, Shi S, Wang R, et al. Copper metal-organic frameworks loaded on chitosan film for the efficient inhibition of bacteria and local infection therapy. *Nanoscale* 2019;11:11830–8.
- [14] Xu X, Lu Y, Li S, Guo S, He M, Luo K, et al. Copper-modified Ti6Al4V alloy fabricated by selective laser melting with pro-angiogenic and anti-inflammatory properties for potential guided bone regeneration applications. *Mater Sci Eng C* 2018;90:198–210.
- [15] Peng C, Zhang S, Sun Z, Ren L, Yang K. Effect of annealing temperature on mechanical and antibacterial properties of Cu-bearing titanium alloy and its preliminary study of antibacterial mechanism. *Mater Sci Eng C Mater Biol Appl* 2018;93:495–504.
- [16] Guo S, Lu Y, Wu S, Liu L, He M, Zhao C, et al. Preliminary study on the corrosion resistance, antibacterial activity and cytotoxicity of selective-laser-melted Ti6Al4V-x Cu alloys. *Mater Sci Eng C* 2017;72:631–40.
- [17] Abdallah MN, Tran SD, Abughanam G, Laurenti M, Zuanazzi D, Mezour MA, et al. Biomaterial surface proteomic signature determines interaction with epithelial cells. *Acta Biomater* 2017;54:150–63.
- [18] Groen N, Guvendiren M, Rabitz H, Welsh WJ, Kohn J, de Boer J. Stepping into the omics era: opportunities and challenges for biomaterials science and engineering. *Acta Biomater* 2016;34:133–42.
- [19] Wisniewski JR, Zougman A, Nagaraj N, Mann M. Universal sample preparation method for proteome analysis. *Nat Methods* 2009;6:359–62.
- [20] Liu R, Tang Y, Zeng L, Zhao Y, Ma Z, Sun Z, et al. In vitro and in vivo studies of antibacterial copper-bearing titanium alloy for dental application. *Dent Mater* 2018;34:1112–26.
- [21] Haenle M, Zietz C, Lindner T, Arndt K, Vetter A, Mittelmeier W, et al. A model of implant-associated infection in the tibial metaphysis of rats. *Scientific World J* 2013;2013:481975.
- [22] Yang J, Zhang K, Zhang S, Fan J, Guo X, Dong W, et al. Preparation of calcium phosphate cement and polymethyl methacrylate for biological composite bone cements. *Med Sci Monit* 2015;21:1162–72.
- [23] Liu R, Memarzadeh K, Chang B, Zhang Y, Ma Z, Allaker RP, et al. Antibacterial effect of copper-bearing titanium alloy (Ti-Cu) against *Streptococcus mutans* and *Porphyromonas gingivalis*. *Sci Rep* 2016;6:29985.
- [24] D'Mello S, Elangovan S, Hong L, Ross RD, Sumner DR, Salem AK. Incorporation of copper into chitosan scaffolds promotes bone regeneration in rat calvarial defects. *J Biomed Mater Res B Appl Biomater* 2015;103:1044–9.
- [25] Wu C, Zhou Y, Xu M, Han P, Chen L, Chang J, et al. Copper-containing mesoporous bioactive glass scaffolds with multifunctional properties of angiogenesis capacity, osteostimulation and antibacterial activity. *Biomaterials* 2013;34:422–33.
- [26] Bari A, Bloise N, Fiorilli S, Novajra G, Vallet-Regí M, Bruni G, et al. Copper-containing mesoporous bioactive glass nanoparticles as multifunctional agent for bone regeneration. *Acta Biomater* 2017;55:493–504.
- [27] Glenske K, Donkiewicz P, Köwitsch A, Milosevic-Oljaca N, Rider P, Rofall S, et al. Applications of metals for bone regeneration. *Int J Mol Sci* 2018;19:826.
- [28] Borland SJ, Morris TG, Borland SC, Morgan MR, Francis SE, Merry C, et al. Regulation of vascular smooth muscle cell calcification by syndecan-4/FGF-2/PKC α signalling and cross-talk with TGF β . *Cardiovasc Res* 2017;113:1639–52.
- [29] Banyai L, Sonderegger P, Patthy L. Agrin binds BMP2, BMP4 and TGF β 1. *PLoS One* 2010;5:e10758.
- [30] Zimmermann N, Saiga H, Houthuys E, Moura-Alves P, Koehler A, Bandermann S, et al. Syndecans promote mycobacterial internalization by lung epithelial cells. *Cell Microbiol* 2016;18(12):1846–56. 2016-12-01.
- [31] Magalhaes A, Marcos NT, Carvalho AS, David L, Figueiredo C, Bastos J, et al. *Helicobacter pylori* cag pathogenicity island-positive strains induce syndecan-4 expression in gastric epithelial cells. *FEMS Immunol Med Microbiol* 2009;56(3):223–32. 2009-08-01.
- [32] Zhang J, Wang Y, Chu Y, Su L, Gong Y, Zhang R, et al. Agrin is involved in lymphocytes activation that is mediated by alpha-dystroglycan. *FASEB J* 2006;20(1):50–8. 2006-01-01.
- [33] Trautmann A, Vivier E. Immunology. Agrin—a bridge between the nervous and immune systems. *Science* 2001;292(5522):1667–8. 2001-06-01.